10-24-2013

Reactive Pathways in the Chlorobenzene–Ammonia Dimer Cation Radical: New Insights from Experiment and Theory

Scott Reid
Marquette University, scott.reid@marquette.edu

Journal of Physical Chemistry : A, Vol. 117, No. 47 (November 27, 2013): 12429–12437. DOI.

Reactive Pathways in the Chlorobenzene–Ammonia Dimer Cation Radical: New Insights from Experiment and Theory

Scott A. Reid
Department of Chemistry, Marquette University, Milwaukee, Wisconsin
Silver Nyambo
Department of Chemistry, Marquette University, Milwaukee, Wisconsin
Aimable Kalume
Department of Chemistry, Marquette University, Milwaukee, Wisconsin
Brandon Uhler
Department of Chemistry, Marquette University, Milwaukee, Wisconsin
Cyrus Karshenas
Department of Chemistry, Marquette University, Milwaukee, Wisconsin
Lloyd Muzangwa
Department of Chemistry, Marquette University, Milwaukee, Wisconsin

Abstract

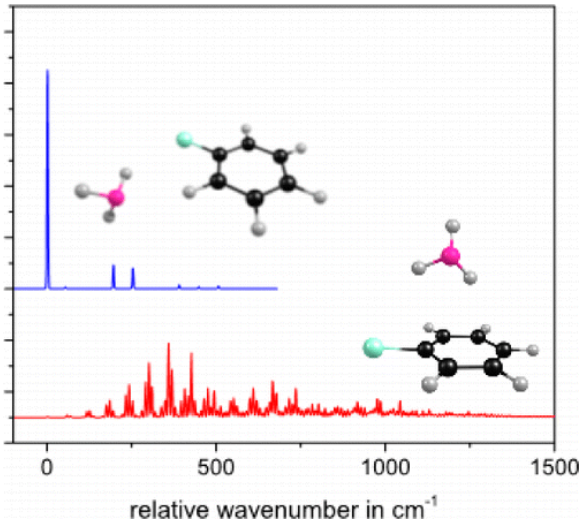

Building upon our recent studies of noncovalent interactions in chlorobenzene and bromobenzene clusters, in this work we focus on interactions of chlorobenzene (PhCl) with a prototypical N atom donor, ammonia (NH_3). Thus, we have obtained electronic spectra of PhCl···$(NH_3)_n$ (n = 1–3) complexes in the region of the PhCl monomer S_0 −S_1 ($\pi\pi^*$) transition using resonant 2-photon ionization (R2PI) methods combined with time-of-flight mass analysis. Consistent with previous studies, we find that upon ionization the PhCl···NH_3 dimer cation radical reacts primarily via Cl atom loss. A second channel, HCl loss, is identified for the first time in R2PI studies of the 1:1 complex, and a third channel, H atom loss, is identified for the first time. While prior studies have assumed the dominance of a π-type complex, we find that the reactive complex corresponds instead to an in-plane σ-type complex. This is supported by electronic structure calculations using density functional theory and post-Hartree–Fock methods and Franck–Condon analysis. The reactive pathways in this system were extensively characterized computationally, and consistent with results from previous calculations, we find two nearly isoenergetic arenium ions (Wheland intermediates; denoted WH1, WH2), which lie energetically below the initially formed dimer cation radical complex. At the energy of our experiment, intermediate WH1, produced from *ipso*-addition, is not stable with respect to Cl or HCl loss, and the relative branching between these channels observed in our experiment is well reproduced by microcanonical transition state theory calculations based upon the calculated parameters. Intermediate WH2, where NH_3 adds ortho to the halogen, decomposes over a large barrier via H atom loss to form protonated *o*-chloroaniline. This channel is not open at the (2-photon) energy of our experiments, and it is suggested that photodissociation of a long-lived (i.e., several ns) WH2 intermediate leads to the observed products.

I Introduction

The study of molecular clusters offers valuable insight into important noncovalent interactions including hydrogen bonding, π–π stacking, CH/π interactions, and halogen bonding. These fall into a general class of donor–acceptor interactions and are important in many chemical and biological processes. For example, such interactions play an important role in controlling chemical reactivity and molecular structure,(1-10) are central to processes of molecular recognition and binding,(11-16) and contribute to the structure and function of biomolecules.(17-22) Increasingly, halogen-bonding has been recognized as an important noncovalent interaction in systems featuring halogen atoms.(3, 15, 23-30) The halogen bond, which involves a halogen (X) atom as electron acceptor, arises from the polarized electron distribution around the halogen, which gives rise to a region of positive electrostatic potential on the axis of the C–X bond referred to as the “σ-hole”.(31-33) The

magnitude of this hole depends both on the halogen, increasing from F to I, and electron withdrawing power of substituent groups.(34)

Because of the presence of a convenient chromophore, which allows the application of one-color resonant 2-photon ionization (R2PI) spectroscopy with mass-selective detection, clusters of aromatics have long been used as model systems for probing noncovalent interactions of various types.(35, 36) In early studies by Zwier and co-workers,(37, 38) the water–benzene complex was detected using R2PI spectroscopy in concert with resonant ion dip infrared spectroscopy. The data supported a π-type structure for the complex, which, however, was determined in model calculations to be extremely floppy. In the ensuing years, ionization based methods have been extensively applied to the study of molecular complexes.(39-81)

The dimers of halobenzenes with ammonia are model systems for understanding the effects of complex formation on bimolecular reactions, as found initially by Brutschy and co-workers.(82, 83) In a 1988 communication and a later report in 1990, Maeyama and Mikami showed that ionization of the $PhCl\cdots NH_3$ complex resulted in Cl atom loss to yield protonated aniline (anilinium ion), through an intracluster S_N2 reaction from the ionized complex.(76) The origin band of the S_0–S_1 spectrum of the complex was blue-shifted from the monomer (PhCl) origin by ∼76 cm^{-1}, and while no information on the structure of the complex was obtained, the following reaction scheme was postulated:

(1)

$$\begin{aligned} C_6H_5Cl\cdots NH_3 \xrightarrow{2h\nu} & \quad [C_6H_5Cl\cdots NH_3]^{+\bullet} \\ \rightarrow & \quad [C_6H_5Cl-NH_3]^{+\bullet} \\ \rightarrow & \quad [C_6H_5NH_3]^{+} + Cl^{\bullet} \end{aligned}$$

Brutschy and co-workers conducted similar R2PI studies on fluorobenzene, chlorobenzene, and *p*-chlorofluorobenzene complexes with methanol and ammonia.(77-83) In the case of the $PhF\cdots NH_3$ dimer, a blue-shifted (∼58 cm^{-1}) feature was observed in the S_0–S_1 spectrum, but the dimer was found to be unreactive upon ionization. This was consistent with earlier biomolecular reactions of halobenzene cations with ammonia, where PhX (X = Cl, Br, I) radical cations were found to react with ammonia to yield anilinium ions, but PhF radical cations did not.(84) However, the $PhF\cdots(NH_3)_2$ complex did react upon ionization, decaying via either HF loss, to give the aniline cation radical, or dissociative electron transfer. A band observed ∼47 cm^{-1} above the S_1 origin of the 1:1 dimer was initially assigned to the 1:2 dimer; however, this assignment was later questioned, and this band attributed to a second conformer of the 1:1 dimer.(85) In a more recent study by Cockett and co-workers, which employed multidimensional Franck–Condon simulations,(86) it was shown that the structure in the S_0–S_1 spectrum can be attributed solely to an in-plane four-center σ_{ortho} complex, bound by C–H···N and N–H···F interactions.

In 2006, Brutschy and co-workers published IR-depletion spectroscopy in the N–H stretching region of NH_3 clusters with benzene, toluene, fluorobenzene, chlorobenzene, and *p*-difluorobenzene;(87) the spectra were complemented by theoretical studies at the MP2 level. For the halobenzenes, MP2 calculations identified three isomers of the 1:1 complex with ammonia; (a) a structure bound solely by N–H/π interaction with one N–H group pointing into the π-cloud of the halobenzene (π_{out}), (b) a structure bound by both N–H/π interaction and a N–H···Cl hydrogen bond (π_{bridge}); and (c) an in-plane, four-center structure bound by N···H–C and N–H···Cl hydrogen bonds (σ_{ortho}). By comparing the experimental shifts from the free NH_3 absorptions, the authors concluded that the observed structure of the $PhF\cdots NH_3$ and $PhCl\cdots NH_3$ clusters corresponded to the out-of-plane (π_{bridge}) structure. This stands in contrast with the findings of Cockett and co-workers for $PhF\cdots NH_3$.(86) While an above plane (π-type) complex could be envisioned to easily react upon ionization, does the reactive dimer for

PhCl···NH_3 correspond to an in-plane structure? This is one of the questions we seek to address in the present study.

Information on the binding energy of PhCl···$(NH_3)_n$ clusters comes from the study of Garvey and co-workers, who used tunable VUV radiation to effect single-photon ionization.(88) The ionization potentials of the PhCl···$(NH_3)_n$ clusters with n = 1–3 were measured, and from the appearance potentials, the dissociation energy of the PhCl···NH_3 dimer was determined to be 12.2 ± 2.2 kJ/mol, while that of the $[PhCl\cdots NH_3]^{+\bullet}$ cation radical was found to be 43.5 ± 2.9 kJ/mol. Importantly, this study identified a second loss channel for the ionized dimer, HCl loss giving rise to the aniline cation radical, which was suggested to come from the ionized dimer and not from secondary processes. To date this channel has not been seen in R2PI studies; however, it is noteworthy that a molecular elimination channel forming HCl was observed in R2PI studies of PhClF···NH_3 clusters by Brutschy and co-workers.(80, 89)

The prototypical PhCl + NH_3 system has also been the subject of theoretical investigation. Early MNDO calculations predicted a triple-well energy profile, with reaction from the initial ionized complex leading through *ipso*-substitution to a chlorocyclohexadienyl radical ion, or Wheland intermediate, the loss of Cl from which proceeded without a barrier to give the Cl + protonated aniline products.(84) At this level of theory, the intermediate was calculated to lie 34 kJ/mol below the ionized complex. Such intermediates in related systems have been the focus of recent experimental studies.(90-92) More recently, Tachikawa examined ionization processes in the PhCl···NH_3 complex using direct ab initio molecular dynamics.(93) In this work, the complex was presumed to adopt a π_{out} structure, and two Wheland intermediates were found, which computationally were formed in nearly equal yield following a vertical photoionization. The first resulted from *ipso*-substitution (we denote this WH1 throughout this work), the second from substitution ortho to the halogen (WH2). At energies corresponding to a vertical ionization, WH1 was formed within ∼0.5 ps following ionization, and Cl atom loss followed on a ∼1 ps time scale. In contrast, while WH2 was formed on a similar time scale, it exhibited a longer lifetime (>2 ps) due to the high barrier for C–H bond fission. There has to date been no experimental evidence for the formation of WH2.

Despite the many studies on this prototypical system, it is clear that significant open questions remain, particularly concerning the structure of the reactive complex. Moreover, to date, halogen bonded structures have not been considered. Building upon previous studies of noncovalent interactions in chlorobenzene clusters, the present work highlights the study of clusters of chlorobenzene with ammonia. Experimental studies using R2PI spectroscopy are supported by electronic structure calculations based upon density functional theory (DFT) and post-Hartree–Fock (MP2) methods in concert with correlation consistent basis sets, which have characterized the important stationary points and reactive pathways in this prototypical system. While prior studies have assumed the dominance of a π-type complex, we find that the reactive complex corresponds instead to an in-plane σ-type complex. The reactive pathways in this system were extensively characterized computationally, and consistent with results from previous calculations, we find two nearly isoenergetic arenium ions (Wheland intermediates; denoted WH1, WH2), which lie energetically below the initially formed dimer cation radical. At the energy of our experiment, intermediate WH1, produced from *ipso*-addition, is not stable with respect to Cl or HCl loss, and the relative branching between these channels observed in our experiment is well reproduced by microcanonical transition state theory calculations based upon the calculated parameters.

II Experimental and Computational Methods

Our experiments utilized a linear time-of-flight mass spectrometer (TOFMS) coupled with a supersonic molecular beam source. A 1:5:100 mixture of chlorobenzene/NH_3/He was generated by passing a premix of NH_3/He over a sample of chlorobenzene held in a temperature controlled bath. This mixture was expanded at a total pressure

of typically ∼1–2 bar from the 1.0 mm diameter nozzle of a solenoid-activated pulsed valve (General Valve), and the resulting gas pulse, of ∼1 ms duration, passed through a 1.0 mm diameter skimmer into the differentially pumped flight tube of a one-meter linear TOFMS. The flight tube vacuum was maintained by a 250 L/s turbomolecular pump, and a gate valve used to isolate the detector, which was kept under vacuum at all times. The main chamber was evacuated with a water-baffled diffusion pump (Varian VHS-4). With the nozzle on, typical pressures were $\sim 5 \times 10^{-5}$ mbar (main chamber) and $\sim 1 \times 10^{-6}$ mbar (flight tube). The background pressure in the flight tube could be lowered further by liquid nitrogen cooling of the vacuum shroud; however, this was not required in the present experiments.

Ionization was initiated by a 1 + 1 R2PI scheme, with laser light near 270 nm generated from frequency doubling in a BBO crystal the output of a dye laser (Lambda-Physik, Scanmate 2E), pumped by the third harmonic of an Nd:YAG laser (Continuum NY-61). The laser was operated on a C540A dye, giving typical output pulse energies of ∼1 mJ in the doubled beam, which was loosely focused with a 1.0 m plano-convex lens into the chamber.

Ions were extracted and accelerated using a conventional three-plate stack, with the repeller plate typically held at +2100 V, the extractor plate at +1950 V, and the third plate at ground potential.(91) The ions traversed a path of 1 m prior to striking a dual chevron Microchannel Plate (MCP) detector. The detector signal was amplified (×25) using a fast preamplifier (Stanford Research SRS445A), and integrated using a boxcar system (Stanford Research SRS250) interfaced to a personal computer. An in-house LABVIEW program controlled data acquisition and stepped the laser wavelength; typically, the signal from 20 laser shots was averaged at each step in wavelength.

To support our experimental findings, electronic structure calculations were performed using the Gaussian 09 software package on the MU Pere high speed cluster.(94) Full geometry optimizations were carried out using DFT (M06-2X) with an aug-cc-pVDZ basis set, with single-point CCSD(T) energies obtained for selected structures. Prior computational studies on related systems(17, 95, 96) have extensively benchmarked the performance of DFT methods against high level post-Hartree–Fock ab initio single reference methods. The Minnesota meta-GGA (generalized gradient approximation) hybrid functional M06-2X, among other methods, provides a good cost to performance ratio,(97) and the aug-cc-pVDZ basis set performs well in calculating the counterpoise correction.(95) Our calculated binding energies were corrected for zero-point energy (ZPE), with the counterpoise method used to correct for basis set superposition error (BSSE).

Time-dependent DFT (TDDFT) methods based on range-separated hybrid and meta-GGA hybrid functionals were used to calculate the electronic spectra of the clusters and the optimized geometry of the S_1 states. Methods employed included the meta-GGA hybrid functionals M06 and M06-2X,(97) and CAM-B3LYP,(98, 99) all with an aug-cc-pVDZ basis set. The performance of M06-2X for electronic excitations, including Rydberg and Charge Transfer excitations, has recently been benchmarked.(100)

III Results and Discussion

Previous R2PI studies have shown that the PhCl···NH_3 complex displays an origin band, which is shifted ∼76 cm^{-1} to the blue of the S_0–S_1 ($\pi\pi^*$) origin band of the PhCl monomer. With the laser tuned to this position, a representative mass spectrum was obtained and is shown in the lower panel of Figure 1. The upper panel displays an expanded view in the region of the PhCl···NH_3 dimer. Note the small intensity of the parent dimer peak with respect to the higher order clusters, and the strong intensity of daughter peaks corresponding to aniline (An) and protonated aniline (AnH). This is evidence that the dimer, upon ionization, reacts via the following pathways, in addition to the previously mentioned Cl atom loss (1):

(1)

$$C_6H_5Cl\cdots NH_3 \xrightarrow{2h\nu} [C_6H_5Cl\cdots NH_3]^{+\bullet}$$
$$\rightarrow [C_6H_5Cl - NH_3]^{+\bullet}$$
$$\rightarrow [C_6H_5NH_3]^{+} + Cl^{\bullet}$$

(2)

$$\rightarrow [C_6H_5NH_2]^{+\bullet} + HCl$$

(3)

$$\rightarrow [C_6H_4ClNH_3]^{+} + H^{\bullet}$$

Channels 1 and 2 have previously been examined in detail; however, the nature of the intermediate has not been well determined. For example, it is not known whether the Cl and HCl products arise from the same or different intermediates. To our knowledge, no previous reports have identified a channel for H atom loss.

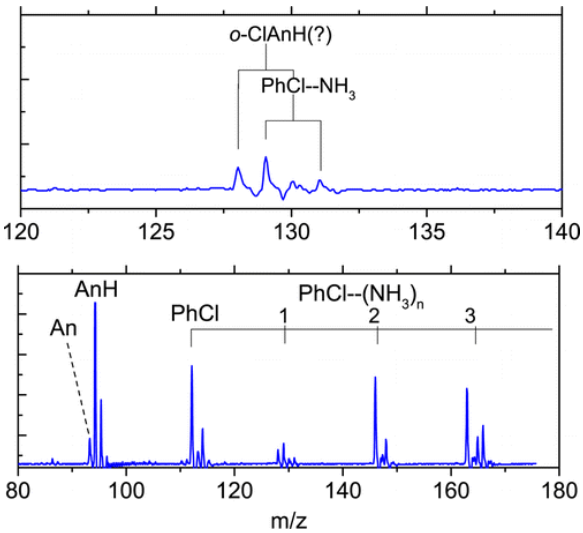

Figure 1. Time-of-flight mass spectrum resulting from resonant 2-photon ionization (R2PI) at a wavelength coincident with the origin band of the PhCl···NH_3 dimer. The small signal at the parent wavelength reflects an intracluster reaction upon ionization, leading to (a) Cl atom loss, producing protonated aniline; (b) HCl loss, producing aniline cation radical; and (c) H atom loss, producing *o*-chloroaniline cation radical.

The R2PI spectrum obtained in the AnH^+ channel, corresponding to Cl atom loss, is compared in the upper panel of Figure 2 with the monomer spectrum. As previously reported, the origin of the complex is shifted ~76 cm^{-1} to the blue of the monomer origin, and the spectrum is origin dominated. These points will be discussed further below. The spectrum in Figure 2 is very similar to those measured in the mass channels associated with aniline and the parent complex, as shown in Figure S1 in the Supporting Information,(101) indicating that these share a common precursor. Our spectra indicate that the 1:1 complex is responsible for this feature, as the R2PI spectra of the 1:2 and 1:3 complexes display very broad, unresolved bands that are most likely indicative of multiple conformers, as shown in Figure S2 in the Supporting Information.

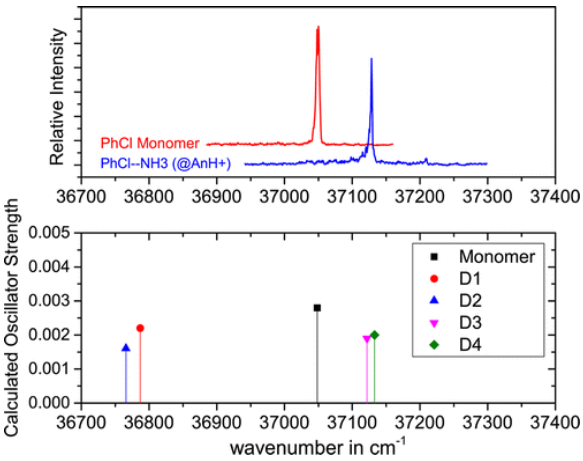

Figure 2. Upper panel: R2PI spectra of the PhCl monomer (red) and PhCl···NH_3 dimer (blue). The latter was measured in the protonated aniline mass channel. Lower panel: Calculated adiabatic transition energies of the PhCl monomer and four minimum energy dimer structures (D1–D4) from TDM06-2X/aug-cc-pVTZ optimizations of the S_0 and S_1 states, scaled to match the experimental value of the monomer absorption.

The prior theoretical (MP2) study of Brutschy and co-workers identified three isomers of the 1:1 complex; π_{out}, π_{bridge}, and σ_{ortho}.(87) To further characterize this complex, we employed DFT calculations at the M06-2X/aug-cc-pVXZ (X = D,T) level, with geometry optimizations initiated from a variety of starting geometries. Our choice of functional stems from the extensive benchmarking reported by Sherrill and co-workers on similar types of complexes.(95) Four minimum energy structures (D1–D4) were found, and these are shown in Figure 3; noted are the calculated binding energies, counterpoise and ZPE corrected, which are similar at this level of theory. Dimers D1, D2, and D3 correspond to previously identified π_{out}, π_{bridge}, and σ_{ortho} structures, while D4 is a second σ complex where the NH_3 group has rotated to afford two N–H···Cl hydrogen bonds. No minimum associated with a halogen-bonded (i.e., C–Cl···N) structure was found at this level of theory. We subsequently carried out single-point counterpoise-corrected CCSD(T)//M06-2X/aug-cc-pVTZ calculations, and these energies are given in Table 1. At this level of theory, D3 is the global minimum energy structure, with a binding energy of −8.0 kJ/mol. This may be compared with the experimental value of −12.0 ± 2.2 kJ/mol.(88)

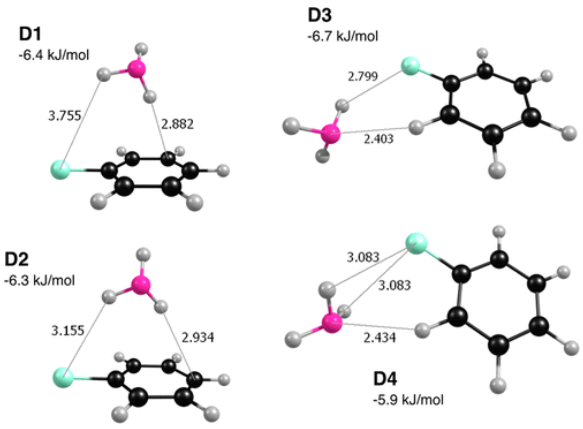

Figure 3. Optimized structures and binding energies of four minimum energy PhCl···NH_3 dimer structures (D1–D4) at the M06-2X/aug-cc-pVTZ level.

Table 1. Calculated Binding Energies of PhCl···NH_3 Dimer Structures

	calculated binding energies (kJ/mol)	
dimer	**M06-2X/aug-cc-pVTZ**	**CCSD(T)//M06-2X/aug-cc-pVTZ**

D1	–6.4	–5.6
D2	–6.7	–4.2
D3	–6.3	–8.0
D4	–5.9	–7.3

Given the range of possible dimer structure(s), which are responsible for the observed electronic spectrum? To answer this question, we carried our TDDFT calculations of the vertical excitation energies, and TDDFT optimizations of S_1 excited states, at the TDCAM-B3LYP and TDM06-2X level of theory, with aug-cc-pVXZ (X = D,T) basis sets. Then, multidimensional Franck–Condon calculations were employed to simulate the vibronic structure in the electronic spectrum, based on the calculated parameters. The adiabatic transition energies obtained from TDM06-2X/aug-cc-pVTZ calculations are shown in the lower panel of Figure 2, where the calculated energies have been scaled to match the experimental energy of the monomer origin.

These calculations predict a red shift for dimers D1 and D2, which involve significant N–H/π interactions, and a blue shift for D3 and D4. The calculated shifts for D3 and D4 are of similar magnitude, and within 10 cm^{-1} of the experimentally observed shift. Thus, while the electronic spectra cannot distinguish between D3 and D4, our results strongly suggest that the observed electronic absorption is associated with a σ-type neutral complex.

Additional evidence in support of this assignment comes from multidimensional Franck–Condon simulations based upon the calculated equilibrium geometries and mass-weighted normal mode displacements, where the effects of Duschinsky mixing were incorporated. The simulations included the lowest frequency intermolecular modes, and representative spectra were calculated for dimers D2 (π-type) and D3 (σ-type). For D3, our calculations find little geometry change between S_0 and S_1, giving rise to origin dominated spectra, as shown in Figure 4, where transitions involving the five lowest frequency intermolecular modes were included. In contrast, D2 undergoes a significant geometry change in the electronic transition, where the N–H···Cl interaction is largely broken in the excited state and a bidentate interaction with the π-system is the preferred binding motif. As a result, extensive FC activity is predicted in the low-frequency intermolecular vibrations (Figure 4), a result inconsistent with the experimental spectrum (Figure 2). Thus, FC simulations also support the assignment of the observed spectrum to a σ-type complex.

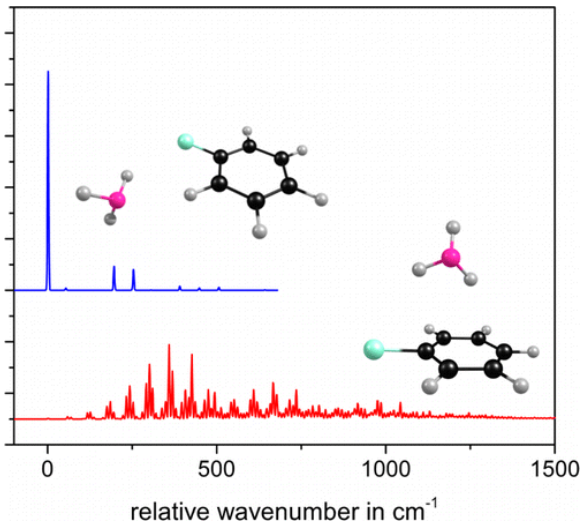

Figure 4. Franck–Condon simulations of the electronic absorptions of the PhCl···NH_3 dimers D2 (lower) and D3. The simulations account for the effects of Dushinsky mixing; details are provided in the text.

Having established though electronic structure calculations and Franck–Condon simulations that a σ-type complex is responsible for the experimental R2PI spectra, we carried out additional calculations on the ionized complex to chart the reaction pathways leading to the observed products. In these calculations we considered two types of Wheland intermediates: one derived from *ipso*-substitution (WH1), the other from substitution at a position ortho to the halogen atom (WH2). The rationale for considering substitution at the ortho as opposed to meta or para positions is the expectation that the structure of D3 should favor the former (Figure 3).

Considering the Wheland intermediate derived from *ipso*-substitution, calculations at the M06-2X/aug-cc-pVDZ level show that WH1 lies 30 kJ/mol lower than the ionized complex (D3), as shown in Figure 5a. While a transition state between D3 and WH1 was not identified computationally, Garvey and co-workers used tunable VUV photoionization to determine the ionization potential of the PhCl···NH_3 dimer as 8.744 ± 0.022 eV, and the appearance potential of protonated aniline (formed coincidentally with Cl atom) as 8.935 ± 0.004 eV,(88) implying a barrier to reaction of ∼14 kJ/mol. A transition state connecting WH1 to the products associated with Cl atom loss (i.e., Cl + protonated aniline) was found computationally and verified by intrinsic reaction coordinate calculations (Figure S3 in Supporting Information). This transition state lies ∼15 kJ/mol above WH1 (Figure 5a). Thus, upon ionization of the complex, *ipso*-substitution leading to WH1 affords C–Cl bond scission to yield protonated aniline.

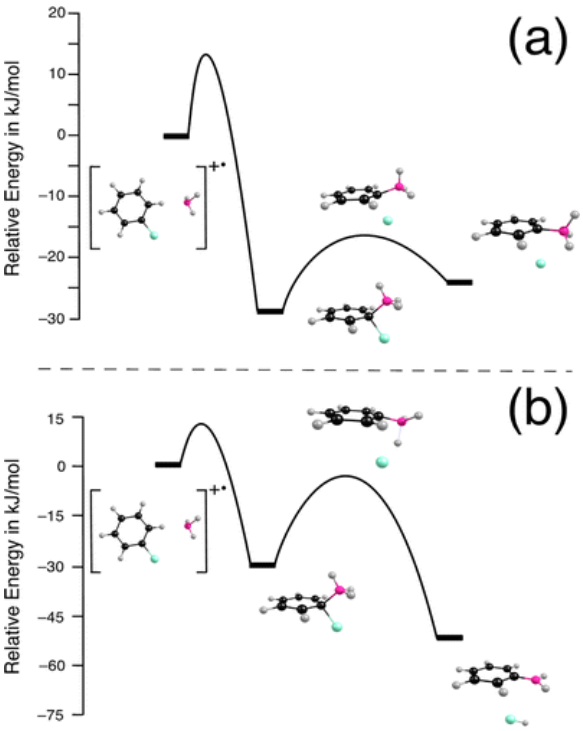

Figure 5. Calculated (M06-2X/aug-cc-pVDZ) stationary points on the potential energy surface of the ionized PhCl···NH_3 complex, reflecting *ipso*-substitution leading to Wheland intermediate WH1. (a) Stationary points associated with the reaction path to Cl atom loss. (b) Stationary points associated with the reaction path to HCl elimination.

Does the HCl elimination channel derive from the same (WH1) intermediate? Theory suggests that it does. As shown in Figure 5b, a four-center transition state leading to the products associated with HCl loss (i.e., HCl + aniline cation radical) was found, as verified by intrinsic reaction coordinate calculations (Figure S4 in Supporting Information). The nature of the reaction path suggests that HCl elimination reflects a frustrated Cl loss from WH1 (Figure 4). It is therefore not surprising that this transition state lies energetically higher than that for Cl loss, ∼25 kJ/mol above WH1 (Figure 5b), yet still lower than the energy of the ionized complex (D3). Thus, *ipso*-

substitution leading to WH1 will afford HCl elimination to yield the aniline cation radical, as is observed (Figure 1).

Theory suggests that the HCl elimination and Cl atom loss channels occur competitively from WH1, yet due to the lower barrier the latter channel should predominate (Figure 5). To quantify the relative branching, we used microcanonical transition state theory as implemented in the CHEMRATE program.(102) On the basis of the transition state structures, vibrational frequencies, and stationary point energies determined from our computational studies, these calculations predict that at the excess energy of our experiment the ratio of Cl to HCl loss is ∼5.6:1. This is in very good agreement with our experimental finding of 5.4:1, determined from the integrated intensities in the TOF mass spectrum shown in Figure 1. The calculated rates for the Cl and HCl channels as a function of energy are shown in Figure S5 in the Supporting Information, while the parameters used in the rate calculations are listed in Table S1.

We now turn to intermediate WH2 and the pathway for H atom loss. As shown in Figure 6, a transition state was found computationally [M06-2X/aug-cc-pVDZ level], which is consistent with addition to form WH2 from ionized dimer D3. This transition state lies ∼4 kJ/mol above the energy of the ionized dimer. Our calculations confirm that WH2 is a minimum, which lies ∼40 kJ/mol below ionized dimer D3. A second transition state was found computationally, connecting WH2 with the products H + protonated *ortho*-chloroaniline (Figure 6). The IRC calculation for this transition state is shown in Figure S6 in the Supporting Information. Our calculations show that H atom loss occurs over a sizable barrier, and neither the energy of this barrier nor the product asymptote is energetically available at the (2-photon) energy of our experiment. On the basis of the energetics shown in Figure 6, in our experiment WH2, once formed, can only decay back to the ionized complex. Microcanonical transition state calculations based upon the calculated parameters (listed in Table S2, Supporting Information) of WH2 and the transition state for back-isomerization predict that the lifetime of the WH2 intermediate is ∼2.5 ns at the 2-photon energy accessed in our experiment. This lifetime is comparable to our laser pulsewidth, and thus, subsequent photodissociation of the initially formed WH2 intermediate is the probable explanation for our observation of a H-atom loss channel. However, because of the small signals associated with this channel, it was not possible to conduct measurements of the fluence dependence of the ion yield, which might confirm this hypothesis. It would be highly desirable to probe this channel using ion-imaging methods.

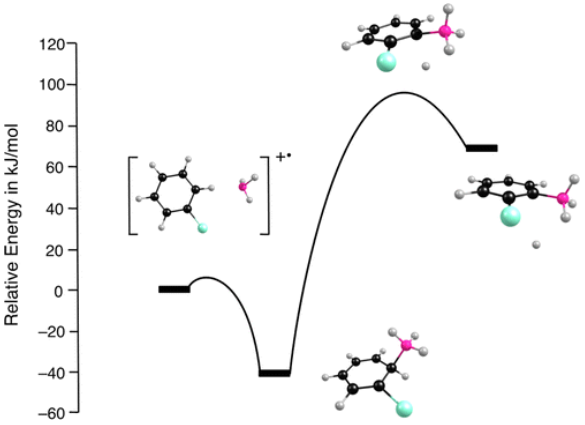

Figure 6. Calculated (M06-2X/aug-cc-pVDZ) stationary points on the potential energy surface of the ionized PhCl···NH_3 complex, reflecting substitution ortho to the halogen, leading to Wheland intermediate WH2. Stationary points associated with the reaction path to H atom loss are shown.

IV Conclusions

In this work, we have examined reactive pathways in a prototypical and well-studied system, the cation radical derived from ionization of chlorobenzene (PhCl) complexed with ammonia (NH_3). R2PI spectra of PhCl···$(NH_3)_n$ (n = 1–3) complexes in the region of the PhCl monomer S_0–S_1 ($\pi\pi^*$) transition find, consistent with earlier studies, that the PhCl···NH_3 dimer cation radical reacts primarily via Cl atom loss, to give protonated aniline. A second channel, HCl loss to give aniline cation radical, is identified for the first time in R2PI studies of the 1:1 complex, and we have also identified a third channel, H atom loss, for the first time. We have shown, both through electronic structure calculations based upon density functional theory and post-Hartree–Fock methods and Franck–Condon analysis, that the reactive complex corresponds to an in-plane σ-type complex. This stands in contrast to previous reports, which have assumed that the neutral dimer structure corresponded to a π-type complex.

In this work, the reactive pathways following photoionization of the complex were extensively characterized computationally. Consistent with a prior direct ab initio molecular dynamics study, two nearly isoenergetic Wheland intermediates were found (WH1 and WH2), which lie significantly lower in energy than the initially formed dimer cation radical. At the energy of our experiment, intermediate WH1, produced from *ipso*-addition, is not stable with respect to Cl or HCl loss, and the branching between these channels is well reproduced by microcanonical transition state theory calculations based on the computed parameters. In contrast, intermediate WH2, where the NH_3 adds ortho to the halogen, decomposes over a large barrier via H atom loss to form protonated *o*-chloroaniline. This channel is not open at the (2-photon) energy of our experiments, and it is suggested that photodissociation of a long-lived WH2 intermediate leads to the observed product.

Supporting Information

Figures S1–S2 show additional R2PI spectra in distinct mass channels for the dimer and higher order complexes. Additional computational data includes intrinsic reaction coordinate calculations for the optimized transition states in this work (Figures S3, S4, and S6). Finally, we include tables of calculated data (Tables S1 and S2) that were used as input into the rate calculations, and a figure displaying the output of those calculations (Figure S5). This material is available free of charge via the Internet at http://pubs.acs.org.

Terms & Conditions

Acknowledgment

Support of this research by the National Science Foundation (CHE-1057951) is gratefully acknowledged. We thank Prof. Rajendra Rathore for many useful discussions. This research was also supported in part by National Science Foundation awards OCI-0923037 ”MRI: Acquisition of a Parallel Computing Cluster and Storage for the Marquette University Grid (MUGrid)” and CBET-0521602 ”Acquisition of a Linux Cluster to Support College-Wide Research & Teaching Activities.”

References

1 Yamakawa, M.; Yamada, I.; Noyori, R. C–H/π Attraction: The Origin of Enantioselectivity in Transfer Hydrogenation of Aromatic Carbonyl Compounds Catalyzed by Chiral Eta(6)-Arene-Ruthenium(II) Complexes Angew. Chem., Int. Ed. **2001**, 40, 2818– 2821

2 Nishio, M. C–H/π Hydrogen Bonds in Organic Reactions Tetrahedron **2005**, 61, 6923– 6950

3 Bertani, R.; Sgarbossa, P.; Venzo, A.; Lelj, F.; Amati, M.; Resnati, G.; Pilati, T.; Metrangolo, P.; Terraneo, G. Halogen Bonding in Metal–Organic-Supramolecular Networks Coord. Chem. Rev. **2010**, 254, 677– 695

4 Nishio, M. The C–H/π Hydrogen Bond: Implication in Chemistry J. Mol. Struct. **2012**, 1018, 2– 7

5 Grabowski, S. J. What Is the Covalency of Hydrogen Bonding? Chem. Rev. **2011**, 111, 2597– 2625

6 Legon, A. C.; Millen, D. J. The Nature of the Hydrogen-Bond to Water in the Gas-Phase Chem. Soc. Rev. **1992**, 21, 71– 78

7 Del Bene, J. E.; Jordan, M. J. T. Vibrational Spectroscopy of the Hydrogen Bond: An ab Initio Quantum-Chemical Perspective Int. Rev. Phys. Chem. **1999**, 18, 119– 162

8 Pimentel, G. C.; McClellan, A. L. The Hydrogen Bond; W.H. Freeman; New York, 1960.

9 Schuster, P.; Zundel, G.; Sandorfy, C. The Hydrogen Bond: Recent Developments in Theory and Experiments; North-Holland Publishing Company: Amsterdam, The Netherlands, 1976.

10 Smith, D. A. Division of Computers in Chemistry. In Modeling the Hydrogen Bond; 206th Meeting of the American Chemical Society, Chicago IL; American Chemical Society: Washington, DC, 1994.

11 Muraki, M. The Importance of C–H/π Interactions to the Function of Carbohydrate Binding Proteins Protein Peptide Lett. **2002**, 9, 195– 209

12 Nakagawa, Y.; Irie, K.; Yanagita, R. C.; Ohigashi, H.; Tsuda, K. Indolactam-V Is Involved in the C–H/π Interaction with Pro-11 of the Pkc Delta C1b Domain: Application for the Structural Optimization of the Pkc Delta Ligand J. Am. Chem. Soc. **2005**, 127, 5746– 5747

13 Ramirez-Gualito, K.; Alonso-Rios, R.; Quiroz-Garcia, B.; Rojas-Aguilar, A.; Diaz, D.; Jimenez-Barbero, J.; Cuevas, G. Enthalpic Nature of the C–H/π Interaction Involved in the Recognition of Carbohydrates by Aromatic Compounds, Confirmed by a Novel Interplay of NMR, Calorimetry, and Theoretical Calculations J. Am. Chem. Soc. **2009**, 131, 18129– 18138

14 Nishio, M. The CH/π Hydrogen Bond in Chemistry. Conformation, Supramolecules, Optical Resolution and Interactions Involving Carbohydrates Phys. Chem. Chem. Phys. **2011**, 13, 13873– 13900

15 Cavallo, G.; Metrangolo, P.; Pilati, T.; Resnati, G.; Sansotera, M.; Terraneo, G. Halogen Bonding: A General Route in Anion Recognition and Coordination Chem. Soc. Rev. **2010**, 39, 3772– 3783

16 Amendola, V.; Fabbrizzi, L.; Mosca, L. Anion Recognition by Hydrogen Bonding: Urea-Based Receptors Chem. Soc. Rev. **2010**, 39, 3889– 3915

17 Thanthiriwatte, K. S.; Hohenstein, E. G.; Burns, L. A.; Sherrill, C. D. Assessment of the Performance of DFT and DFT-D Methods for Describing Distance Dependence of Hydrogen-Bonded Interactions J. Chem. Theory Comput. **2011**, 7, 88– 96

18 Nishio, M.; Umezawa, Y.; Hirota, M. The C–H/π Interaction. Implications in Molecular Recognition J. Syn. Org. Chem. Jpn. **1997**, 55, 2– 12

19 Auffinger, P.; Hays, F. A.; Westhof, E.; Ho, P. S. Halogen Bonds in Biological Molecules Proc. Natl. Acad. Sci. U.S.A. **2004**, 101, 16789– 16794

20 Voth, A. R.; Hays, F. A.; Ho, P. S. Directing Macromolecular Conformation through Halogen Bonds Proc. Natl. Acad. Sci. U.S.A. **2007**, 104, 6188– 6193

21 Nishio, M.; Hirota, M.; Umezawa, Y. The CH−π Interaction: Evidence, Nature, and Consequences; Wiley: New York, 1998.

22 Desiraju, G. R.; Steiner, T. The Weak Hydrogen Bond: In Structural Chemistry and Biology; Oxford University Press: Oxford, U.K., 1999.

23 Cheng, L.; Wang, M. Y.; Wu, Z. J.; Su, Z. M. Electronic Structures and Chemical Bonding in 4d Transition Metal Monohalides J. Comput. Chem. **2007**, 28, 2190– 2202

24 Lu, Y. X.; Zou, J. W.; Wang, Y. H.; Jiang, Y. J.; Yu, Q. S. Ab Initio Investigation of the Complexes between Bromobenzene and Several Electron Donors: Some Insights into the Magnitude and Nature of Halogen Bonding Interactions J. Phys. Chem. A **2007**, 111, 10781– 10788
25 Lu, Y. X.; Zou, J. W.; Wang, Y. H.; Yu, Q. S. Theoretical Investigations of the C–X/π Interactions between Benzene and Some Model Halocarbons Chem. Phys. **2007**, 334, 1– 7
26 Metrangolo, P.; Meyer, F.; Pilati, T.; Resnati, G.; Terraneo, G. Halogen Bonding in Supramolecular Chemistry Angew. Chem., Int. Ed. **2008**, 47, 6114– 6127
27 Metrangolo, P.; Neukirch, H.; Pilati, T.; Resnati, G. Halogen Bonding Based Recognition Processes: A World Parallel to Hydrogen Bonding Acc. Chem. Res. **2005**, 38, 386– 395
28 Parisini, E.; Metrangolo, P.; Pilati, T.; Resnati, G.; Terraneo, G. Halogen Bonding in Halocarbon-Protein Complexes: A Structural Survey Chem. Soc. Rev. **2011**, 40, 2267– 2278
29 Politzer, P.; Murray, J. S.; Clark, T. Halogen Bonding: An Electrostatically-Driven Highly Directional Noncovalent Interaction Phys. Chem. Chem. Phys. **2010**, 12, 7748– 7757
30 Liu, B. K.; Wang, B. X.; Wang, Y. Q.; Wang, L. Ultrafast Dynamics of Chlorobenzene Clusters Chem. Phys. Lett. **2009**, 477, 266– 270
31 Clark, T.; Hennemann, M.; Murray, J. S.; Politzer, P. Halogen Bonding: The σ-Hole J. Mol. Model. **2007**, 13, 291– 296
32 Politzer, P.; Lane, P.; Concha, M. C.; Ma, Y.; Murray, J. S. An Overview of Halogen Bonding J. Mol. Model. **2007**, 13, 305– 311
33 Politzer, P.; Murray, J. S.; Concha, M. C. Halogen Bonding and the Design of New Materials: Organic Bromides, Chlorides and Perhaps Even Fluorides as Donors J. Mol. Model. **2007**, 13, 643– 650
34 Peralta-Inga, Z.; Murray, J. S.; Politzer, P. Computational Exploration of the Relationship between Interaction Energies, Angles of Interaction and Electrostatic Potentials in a Series of Hydrogen- and Halogen-Bonded Complexes. Abstracts of Papers, 239th ACS National Meeting, San Francisco, CA, March 21–25, 2010; COMP-49.
35 Chipot, C.; Jaffe, R.; Maigret, B.; Pearlman, D. A.; Kollman, P. A. Benzene Dimer: A Good Model for π–π Interactions in Proteins? A Comparison between the Benzene and the Toluene Dimers in the Cas Phase and in an Aqueous Solution J. Am. Chem. Soc. **1996**, 118, 11217– 11224
36 Di Palma, T. M.; Bende, A.; Borghese, A. Photoionisation and Structures of Jet-Formed Toluene Clusters Chem. Phys. Lett. **2010**, 495, 17– 23
37 Augspurger, J. D.; Dykstra, C. E.; Zwier, T. S. Hydrogen-Bond Swapping in the Benzene Water Complex: a Model Study of the Interaction Potential J. Phys. Chem. **1992**, 96, 7252– 7257
38 Pribble, R. N.; Zwier, T. S. Probing Hydrogen-Bonding in Benzene–(Water)(N) Clusters Using Resonant Ion-Dip Ir Spectroscopy Faraday Discuss. **1994**, 97, 229– 241
39 Roithova, J. Characterization of Reaction Intermediates by Ion Spectroscopy Chem. Soc. Rev. **2012**, 41, 547– 559
40 Troxler, T.; Leutwyler, S. Molecular-Dynamics and Semiclassical Electronic-Spectra of Naphthalene-Ar_n Clusters ($n \leq 4$) J. Chem. Phys. **1993**, 99, 4363– 4378
41 Furlan, A.; Leutwyler, S.; Riley, M. J. Intermolecular Perturbation of a Jahn–Teller System: the Triptycene·Ne(n) (n = 1–3) Van-Der-Waals Clusters J. Chem. Phys. **1994**, 100, 840– 855
42 Mandziuk, M.; Bacic, Z.; Droz, T.; Leutwyler, S. Intermolecular Vibrations of the 2,3-Dimethylnaphthalene–Ar Van-Der-Waals Complex: Experiment and Quantum 3-Dimensional Calculations J. Chem. Phys. **1994**, 100, 52– 62
43 Droz, T.; Burgi, T.; Leutwyler, S. State-Selective Analysis of Ground-State Vibrational Predissociation Product of an Aromatic Van-Der-Waals Complex Ber. Bunsen. Phys. Chem. **1995**, 99, 429– 433
44 Pribble, R. N.; Gruenloh, C.; Zwier, T. S. The Ultraviolet and Infrared Spectroscopy of $(Benzene)_2$-$(CH_3OH)_3$ Isomeric Clusters Chem. Phys. Lett. **1996**, 262, 627– 632
45 Yeh, J. H.; Shen, T. L.; Nocera, D. G.; Leroi, G. E.; Suzuka, I.; Ozawa, H.; Namuta, Y. Resonance Two-Photon Ionization Spectroscopy of the Aniline Dimer J. Phys. Chem. **1996**, 100, 4385– 4389

46 Wallimann, F.; Frey, H. M.; Leutwyler, S.; Riley, M. Isotopically Resolved (B)–(X) Electronic Spectrum of Ag_3 and Calculation of Its Jahn–Teller Effects Z. Phys. D **1997**, 40, 30– 35
47 Furlan, A.; Leutwyler, S.; Riley, M. J. Coupling of a Jahn–Teller Pseudorotation with a Hindered Internal Rotation in an Isolated Molecule: 9-Hydroxytriptycene J. Chem. Phys. **1998**, 109, 10767– 10780
48 Gruenloh, C. J.; Carney, J. R.; Hagemeister, F. C.; Arrington, C. A.; Zwier, T. S.; Fredericks, S. Y.; Wood, J. T.; Jordan, K. D. Resonant Ion-Dip Infrared Spectroscopy of the S-4 and D-2d Wafer Octamers in Benzene-$(Water)_8$ and $Benzene_2$-$(Water)_8$ J. Chem. Phys. **1998**, 109, 6601– 6614
49 Knochenmuss, R.; Karbach, V.; Wickleder, C.; Graf, S.; Leutwyler, S. Vibrational-Energy Redistribution and Vibronic Coupling in 1-Naphthol·Water Complexes J. Phys. Chem. A **1998**, 102, 1935– 1944
50 Carney, J. R.; Zwier, T. S. Infrared and Ultraviolet Spectroscopy of Water-Containing Clusters of Indole, 1-Methylindole, and 3-Methylindole J. Phys. Chem. A **1999**, 103, 9943– 9957
51 Bach, A.; Leutwyler, S. Proton Transfer in 7-Hydroxyquinoline·(NH_3)(N) Solvent Clusters J. Chem. Phys. **2000**, 112, 560– 565
52 Gruenloh, C. J.; Carney, J. R.; Hagemeister, F. C.; Zwier, T. S.; Wood, J. T.; Jordan, K. D. Resonant Ion-Dip Infrared Spectroscopy of Benzene-$(Water)_9$: Expanding the Cube J. Chem. Phys. **2000**, 113, 2290– 2303
53 Bach, A.; Tanner, C.; Manca, C.; Frey, H. M.; Leutwyler, S. Ground- and Excited State Proton Transfer and Tautomerization in 7-Hydroxyquinoline-(NH_3)(N) Clusters: Spectroscopic and Time Resolved Investigations J. Chem. Phys. **2003**, 119, 5933– 5942
54 Stearns, J. A.; Zwier, T. S. Infrared and Ultraviolet Spectroscopy of Jet-Cooled *ortho*-, *meta*-, and *para*-Diethynylbenzene J. Phys. Chem. A **2003**, 107, 10717– 10724
55 Tanner, C.; Henseler, D.; Leutwyler, S.; Connell, L. L.; Felker, P. M. Structural Study of the Hydrogen-Bonded 1-Naphthol-$(NH_3)_2$ Cluster J. Chem. Phys. **2003**, 118, 9157– 9166
56 Muller, A.; Frey, J. A.; Leutwyler, S. Probing the Watson–Crick, Wobble, and Sugar-Edge Hydrogen Bond Sites of Uracil and Thymine J. Phys. Chem. A **2005**, 109, 5055– 5063
57 Selby, T. M.; Clarkson, J. R.; Mitchell, D.; Fitzpatrick, J. A. J.; Lee, H. D.; Pratt, D. W.; Zwier, T. S. Isomer-Specific Spectroscopy and Conformational Isomerization Energetics of *o*-, *m*-, and *p*-Ethynylstyrenes J. Phys. Chem. A **2005**, 109, 4484– 4496
58 Frey, J. A.; Leist, R.; Muller, A.; Leutwyler, S. Gas-Phase Watson-Crick and Hoogsteen Isomers of the Nucleobase Mimic 9-Methyladenine-2-pyridone ChemPhysChem **2006**, 7, 1494– 1499
59 Tanner, C.; Thut, M.; Steinlin, A.; Manca, C.; Leutwyler, S. Excited-State Hydrogen-Atom Transfer Along Solvent Wires: Water Molecules Stop the Transfer J. Phys. Chem. A **2006**, 110, 1758– 1766
60 Shubert, V. A.; Baquero, E. E.; Clarkson, J. R.; James, W. H.; Turk, J. A.; Hare, A. A.; Worrel, K.; Lipton, M. A.; Schofield, D. P.; Jordan, K. D.Entropy-Driven Population Distributions in a Prototypical Molecule with Two Flexible Side Chains: *O*-(2-Acetamidoethyl)-*N*-acetyltyramine J. Chem. Phys. **2007**, 127, 234315
61 Baquero, E. E.; James, W. H.; Choi, T. H.; Jordan, K. D.; Zwier, T. S. Single Conformation Spectroscopy of a Flexible Bichromophore: 3-(4-Hydroxyphenyl)-*N*-Benzylpropionamide J. Phys. Chem. A **2008**, 112, 11115– 11123
62 James, W. H.; Baquero, E. E.; Shubert, V. A.; Choi, S. H.; Gellman, S. H.; Zwier, T. S. Single-Conformation and Diastereomer Specific Ultraviolet and Infrared Spectroscopy of Model Synthetic Foldamers: Alpha/Beta-Peptides J. Am. Chem. Soc. **2009**, 131, 6574– 6590
63 LeGreve, T. A.; James, W. H.; Zwier, T. S. Solvent Effects on the Conformational Preferences of Serotonin: Serotonin-$(H_2O)_n$, n=1,2 J. Phys. Chem. A **2009**, 113, 399– 410
64 Ottiger, P.; Frey, J. A.; Frey, H. M.; Leutwyler, S. Jet-Cooled 2-Aminopyridine Dimer: Conformers and Infrared Vibrational Spectra J. Phys. Chem. A **2009**, 113, 5280– 5288
65 Shubert, V. A.; Muller, C. W.; Zwier, T. S. Water's Role in Reshaping a Macrocycle's Binding Pocket: Infrared and Ultraviolet Spectroscopy of Benzo-15-crown-5-$(H_2O)_n$ and 4'-Aminobenzo-15-crown-5-$(H_2O)_n$, n = 1, 2 J. Phys. Chem. A **2009**, 113, 8067– 8079
66 Lobsiger, S.; Frey, H. M.; Leutwyler, S. Supersonic Jet UV Spectrum and Nonradiative Processes of the Thymine Analogue 5-Methyl-2-Hydroxypyrimidine Phys. Chem. Chem. Phys. **2010**, 12, 5032– 5040

67 Dean, J. C.; Buchanan, E. G.; James, W. H.; Gutberlet, A.; Biswas, B.; Ramachandran, P. V.; Zwier, T. S. Conformation-Specific Spectroscopy and Populations of Diastereomers of a Model Monolignol Derivative: Chiral Effects in a Triol Chain J. Phys. Chem. A **2011**, 115, 8464– 8478

68 Heid, C. G.; Ottiger, P.; Leist, R.; Leutwyler, S. The S_1/S_2 Exciton Interaction in 2-Pyridone·6-Methyl-2-pyridone: Davydov Splitting, Vibronic Coupling, and Vibronic Quenching. J. Chem. Phys. **2011**, 135.

69 James, W. H.Evolution of Amide Stacking in Larger Gamma-Peptides: Triamide H-Bonded Cycles J. Phys. Chem. A **2011**, 115, 13783– 13798

70 Kumar, S.; Biswas, P.; Kaul, I.; Das, A. Competition between Hydrogen Bonding and Dispersion Interactions in the Indole-Pyridine Dimer and (Indole)(2)-Pyridine Trimer Studied in a Supersonic Jet J. Phys. Chem. A **2011**, 115, 7461– 7472

71 Kumar, S.; Kaul, I.; Biswas, P.; Das, A. Structure of 7-Azaindole-2-Fluoropyridine Dimer in a Supersonic Jet: Competition between N-H--N and N-H--F Interactions J. Phys. Chem. A **2011**, 115, 10299– 10308

72 Lobsiger, S.; Frey, H. M.; Leutwyler, S.; Morgan, P.; Pratt, D. S_0 and S_1 State Structure, Methyl Torsional Barrier Heights, and Fast Intersystem Crossing Dynamics of 5-Methyl-2-hydroxypyrimidine J. Phys. Chem. A **2011**, 115, 13281– 13290

73 Sinha, R. K.; Lobsiger, S.; Trachsel, M.; Leutwyler, S. Vibronic Spectra of Jet-Cooled 2-Aminopurine--H_2O Clusters Studied by UV Resonant Two-Photon Ionization Spectroscopy and Quantum Chemical Calculations J. Phys. Chem. A **2011**, 115, 6208– 6217

74 Kumar, S.; Mukherjee, A.; Das, A. Structure of Indole--Imidazole Heterodimer in a Supersonic Jet: A Gas Phase Study on the Interaction between the Aromatic Side Chains of Tryptophan and Histidine Residues in Proteins J. Phys. Chem. A **2012**, 116, 11573– 11580

75 Trachsel, M. A.; Lobsiger, S.; Leutwyler, S. Out-of-Plane Low-Frequency Vibrations and Nonradiative Decay in the (1)Pi–Pi* State of Jet-Cooled 5-Methylcytosine J. Phys. Chem. B **2012**, 116, 11081– 11091

76 Maeyama, T.; Mikami, N. Nucleophilic-Substitution within the Photoionized Vanderwaals Complex-Generation of $C_6H_5NH_3^+$ from $C_6H_5Cl^-NH_3$ J. Am. Chem. Soc. **1988**, 110, 7238– 7239

77 Brutschy, B. Reactions in Molecular Clusters Following Photoionization J. Phys. Chem. **1990**, 94, 8637– 8647

78 Eggert, J.; Janes, C.; Wassermann, B.; Brutschy, B.; Baumgartel, H. Nucleophilic-Substitution Reactions in Mixed Organic Clusters after Resonant 2-Photon Ionization Ber. Bunsen. Phys. Chem. **1990**, 94, 1282– 1287

79 Brutschy, B.; Eggert, J.; Janes, C.; Baumgartel, H. Nucleophilic-Substitution Reactions in Molecular Clusters Following Photoionization J. Phys. Chem. **1991**, 95, 5041– 5050

80 Brutschy, B. Ion Molecule Reactions within Molecular Clusters Chem. Rev. **1992**, 92, 1567– 1587

81 Brutschy, B. Chemical-Reactions in Mixed Molecular Clusters, Studied by Resonant 2-Photon Ionization Ber. Bunsen. Phys. Chem. **1992**, 96, 1154– 1161

82 Dimopoulourademann, U.; Rademann, K.; Bisling, P.; Brutschy, B.; Baumgartel, H. A Chemical-Reaction and Charge-Transfer in Heteroclusters of Fluorobenzene Ber. Bunsen. Phys. Chem. **1984**, 88, 215– 217

83 Brutschy, B.; Janes, C.; Eggert, J. Selective Intracluster Ion-Chemistry Studied by Resonant 2-Photon Ionization Spectroscopy Ber. Bunsen. Phys. Chem. **1988**, 92, 435– 437

84 Tholmann, D.; Grutzmacher, H. F. Aromatic-Substitution of Halobenzenes in the Gas-Phase: a Kinetic-Study by FT-ICR Spectrometry Chem. Phys. Lett. **1989**, 163, 225– 229

85 Maeyama, T.; Mikami, N. Intracluster Ion Molecule Reactions within the Photoionized Vanderwaals Complexes of C_6H_5F and NH_3 and with H_2O J. Phys. Chem. **1991**, 95, 7197– 7204

86 Tonge, N. M.; MacMahon, E. C.; Pugliesi, I.; Cockett, M. C. R. The Weak Hydrogen Bond in the Fluorobenzene–Ammonia Van Der Waals Complex: Insights into the Effects of Electron Withdrawing Substituents on Pi Versus in-Plane Bonding J. Chem. Phys. **2007**, 126, 154319

87 Vaupel, S.; Brutschy, B.; Tarakeshwar, P.; Kim, K. S. Characterization of Weak NH−π Intermolecular Interactions of Ammonia with Various Substituted Pi-Systems J. Am. Chem. Soc. **2006**, 128, 5416– 5426

88 Grover, J. R.; Cheng, B. M.; Herron, W. J.; Coolbaugh, M. T.; Peifer, W. R.; Garvey, J. F. Photoionization-Induced Intracluster Reactions of Chlorobenzene/Ammonia Mixed Complexes J. Phys. Chem. **1994**, 98, 7479– 7487

89 Riehn, C.; Lahmann, C.; Brutschy, B. Role of Charge-Transfer in Nucleophilic-Substitution Reactions in Clusters of 1-Fluoro-*N*-chlorobenzene Cations with Ammonia Molecules J. Phys. Chem. **1992**, 96, 3626– 3632

90 Mizuse, K.; Fujii, A.; Mikami, N. Infrared and Electronic Spectroscopy of a Model System for the Nucleophilic Substitution Intermediate in the Gas Phase: The C–N Valence Bond Formation in the Benzene-Ammonia Cluster Cation J. Phys. Chem. A **2006**, 110, 6387– 6390

91 Hasegawa, H.; Mizuse, K.; Hachiya, M.; Matsuda, Y.; Mikami, N.; Fujii, A. Observation of an Isolated Intermediate of the Nucleophilic Aromatic Substition Reaction by Infrared Spectroscopy Angew. Chem., Int. Ed. **2008**, 47, 6008– 6010

92 Mizuse, K.; Suzuki, Y.; Mikami, N.; Fujii, A. Solvation-Induced Sigma-Complex Structure Formation in the Gas Phase: A Revisit to the Infrared Spectroscopy of $[C_6H_6\text{-}(CH_3OH)_2]^+$ J. Phys. Chem. A **2011**, 115, 11156– 11161

93 Tachikawa, H. Intramolecular S_N2 Reaction Caused by Photoionization of Benzene Chloride–NH_3 Complex: Direct ab Initio Molecular Dynamics Study J. Phys. Chem. A **2006**, 110, 153– 159

94 Frisch, M. J.; Trucks, G. W.; Schlegel, H. B.; Scuseria, G. E.; Robb, M. A.; Cheeseman, J. R.; Scalmani, G.; Barone, V.; Mennucci, B.; Petersson, G. A.; Gaussian 09, revision D.01; Gaussian, Inc.: Wallingford, CT, 2009.

95 Burns, L. A.; Vazquez-Mayagoitia, A.; Sumpter, B. G.; Sherrill, C. D. Density-Functional Approaches to Noncovalent Interactions: A Comparison of Dispersion Corrections (DFT-D), Exchange-Hole Dipole Moment (XDM) Theory, and Specialized Functionals J. Chem. Phys. **2011**, 134, 084107

96 Sinnokrot, M. O.; Sherrill, C. D. Highly Accurate Coupled Cluster Potential Energy Curves for the Benzene Dimer: Sandwich, T-Shaped, and Parallel-Displaced Configurations J. Phys. Chem. A **2004**, 108, 10200– 10207

97 Zhao, Y.; Truhlar, D. G. The M06 Suite of Density Functionals for Main Group Thermochemistry, Thermochemical Kinetics, Noncovalent Interactions, Excited States, and Transition Elements: Two New Functionals and Systematic Testing of Four M06-Class Functionals and 12 Other Functionals Theor. Chem. Acc. **2008**, 120, 215– 241

98 Yanai, T.; Tew, D. P.; Handy, N. C. A New Hybrid Exchange-Correlation Functional Using the Coulomb-Attenuating Method (CAM-B3LYP) Chem. Phys. Lett. **2004**, 393, 51– 57

99 Peach, M. J. G.; Helgaker, T.; Salek, P.; Keal, T. W.; Lutnaes, O. B.; Tozer, D. J.; Handy, N. C. Assessment of a Coulomb-Attenuated Exchange-Correlation Energy Functional Phys. Chem. Chem. Phys. **2006**, 8, 558– 562

100 Mardirossian, N.; Parkhill, J. A.; Head-Gordon, M. Benchmark Results for Empirical Post-GGA Functionals: Difficult Exchange Problems and Independent Tests Phys. Chem. Chem. Phys. **2011**, 13, 19325– 19337

101 See Supplementary Material Document No._____ for six figures and two tables of additional data. For information on Supplementary Material, see http://www.aip.org/pubservs/epaps.html.

102 Mokrushin, V.; Tsang, W.ChemRate, version 1.5.8; 2009.